# Precursory microcracking and brittle failure of Latur basalt and migmatite gneiss under compressive loading

**M. V. M. S. Rao[1,*], K. J. Prasanna Lakshmi[1], G. M. Nagaraja Rao[2], K. Vijayakumar[1] and S. Udayakumar[2]**

[1]National Geophysical Research Institute (Council of Scientific and Industrial Research), Hyderabad 500 606, India
[2]National Institute of Rock Mechanics, Kolar Gold Fields 563 117, India

**Microcracking activity which occurs in a phased manner in deforming rock under stress has been monitored successfully in the laboratory using acoustic emission (AE) as a tool. The rock samples tested include a massive basalt and a migmatite gneiss that are obtained from the top and bottom portions respectively, of a very deep borehole (KLR-1) drilled at Latur near the surface rupture zone of the Latur–Killari earthquake. The rock samples were subjected to fracture at a constant stress rate under uniaxial compression. The AE statistical parameters used for the analysis include event and energy release rate, amplitude distribution (*b*-value), cumulative energy and ring down count. The results show that dilatancy occurs early in migmatite gneiss and the rock suffers more damage on account of early crack growth during the pre-peak stress regime compared to the massive basalt which is stronger and showed extensive damage only at the peak stress. However, both the rocks show three distinct phases of microcracking activity, namely primary, secondary and nucleation prior to the extensile brittle failure. The AE statistical behaviour of each individual phase is controlled by the size and density distribution of microcracks in rock as inferred from the AE signatures.**

**Keywords.** Acoustic emission, dilatancy, Latur basement rocks, microcracking.

CONTROLLED laboratory experiments of rock fracture and the analyses of accompanying acoustic emissions (AEs) are considered useful for understanding and explaining the various mechanisms of microcracking activity that precedes and culminates in the final failure of rock. The laboratory studies carried out in the early 60s have reported that many similarities are found to exist between the statistics of AE occurring during the compressive fracture of rock and earthquake activity[1], and several studies have progressed since then on those lines. Following the technological advances made in recent decades with regard to the loading methods (stress application) of rocks, and high-speed multi-channel AE waveform recording and source location systems, it has become possible to make detailed studies of fault nucleation and its growth in rocks that are stressed to fracture under a variety of loading conditions in the laboratory[2–9]. The results obtained are found to be useful to understand the micromechanics of rock fracture and its various influencing factors, and also lend support to the interpretation of natural and induced seismicity[3,5,8,9]. Also, the statistical data of AE (occurrence rate of events, *b*-values, energy counts) which can be obtained with the help of either single or dual channel AE-monitoring systems, have been found useful for studying the evolution of pre-failure microcrcak damage; precursory sequences and fracture behaviour of rock[10–14]. This is possible because the number of AE events is approximately proportional to the number of growing cracks, and the AE amplitudes (or energy) are proportional to the length of the crack growth increments in rocks undergoing compressional deformation and failure[11,12].

In this article, the results of AE statistics of precursory microcracking and brittle failure of a massive basalt and migmatite gneiss rock of Latur basement are compared and discussed. The rock samples were obtained from the top and bottom parts respectively, of a 617 m deep borehole (KLR-1) that was especially core-drilled along with a few shallow-depth boreholes for geophysical studies following the disastrous Killari earthquake ($M_w \sim 6.2$) in Latur District, Maharashtra, India on 29 September 1993. The Killari earthquake is the second largest among the earthquakes that have been occurring frequently in the Deccan Volcanic Province (DVP) over the last four decades, beginning with the Koyna earthquake ($M_w$ 6.3) in December 1967 (ref. 15). But the Killari earthquake had drawn global attention since it had occurred at a shallow depth in an area devoid of any neotectonic activity and historic seismicity, and caused widespread damage[15–18]. Its occurrence has led to some introspection among the earth scientists, and many geological and geophysical studies have progressed since then. Several factors such as reactivation of a segment of an ancient fault zone within a craton based on geologic observations[17]; fluid-

*For correspondence. (e-mail: mvmsrao@gmail.com)

filled zones at shallow depths as inferred from magneto-telluric sounding studies to cause mechanical instability[15], and isostatic imbalance caused by possible erosion of the basalt cover adding further compressive stress in the region[18] are found to contribute to the Killari event. Further the presence of an upward high velocity/density mafic crust in the Latur region has been reported[19]. All these studies indicate that it is necessary to make an in-depth analysis of the entire basement of DVP in Peninsular India to identify the other potential seismogenic structures in such areas. The objective of the present study is to identify, track and analyse the various stages of microcracking activity in some of the basement rocks of Latur by subjecting them to compressive stress under controlled laboratory conditions using AE statistics. The massive basalt and migmatite gneiss rocks that are chosen for the present study would represent the top basalt cover (up to 330 m depth) and the granite–gneiss basement at depths > 500 m of the Latur–Killari area.

## Experimental details

### *Data acquisition and replay of AE*

The rock samples were subjected to fracture under uniaxial compression at a constant stress rate (~ 2 MPa/min) using a 150-Ton MTS 815 servo-controlled testing machine. The stress, strain and AE were recorded concurrently using PC-based systems and following the procedure described in detail by us earlier[20,21]. The strain monitoring was carried out using LVDT transducers until ~ 98% failure stress, while the AE monitoring was carried out until the final failure occurred in the rock. We used a resonant-type AE sensor (frequency 150 kHz) and set a fixed threshold of 45 dB for data acquisition. The multiparameter AE data comprising events, hits, ring-down and energy counts, duration and rise time, and amplitude distribution were recorded using the Spartan System. The recorded AE data files were replayed and processed using Mistras-2001 software. Data reduction and evaluation of the various subsets of AE were carried out at the maximum possible digitization rate of the Mistras system (200 bin resolution) using the graphs displayed on the screen and enabling 'graph expansion' and 'cursor' facilities. The experimental results of the present study have been obtained in the form of AE data versus time-to-failure plots so that the various phases of microcracking activity can be identified, tracked and analysed in detail. The frequency of occurrence of microcracking activity has been inferred from the event rate and energy count rate plots. We have made use of AE event–amplitude distribution plots for the computation of $b$-value using the maximum likelihood method[22] and the formula, $b = (20 \log_{10} e)/(a - a_0)$, described by us earlier[23–25]. The AE cumulative energy count data ($\sum E$) were normalized with respect to the final energy count for obtaining the normalized stress-induced microcrack damage data of the samples tested.

## Results and discussion

### *Rock samples*

The massive basalt cores (dia. 54 mm) were obtained from a depth of 214 m of KLR-1 borehole. The test sample (LB-1) chosen for the present study is quite dense (2.922 g/cm$^3$), highly compact and strong (UCS: 267 MPa). A microscopic examination revealed that it contains large quantities of amphibole and plagioclase. The migmatite gneiss (dia. 42 mm core) was obtained from a depth of 580 m from the same borehole. This represents the gnanite–gneiss basement of Latur area. The test sample (A-1) is a medium-grained rock (grain size 5–7 mm) containing large quantities of plagioclase and quartz, and some amphibole. The density and uniaxial compressive strength of A-1 were found to be 2.825 g/cm$^3$ and 187 MPa respectively (Table 1). It showed higher velocity values and lower Poisson ratio on account of the quartz mineral, which is dominantly present in it (Table 1).

### *Stress–strain behaviour*

The load–deformation data were monitored on-line and the records were obtained until ~ 98% failure stress for both the rocks. The stress–strain plots of the massive basalt (LB-1) and migmatite gneiss (A-1) are shown in Figures 1 and 2 respectively. The onset of dilatancy (inelastic volumetric strain) caused due to the formation of tensile microcracks had commenced at 200 MPa (~ 75% failure stress) for LB-1 (Figure 1). On the other hand, the migmatite gneiss (Sample no. A-1) began to dilate rather early at 125 MPa (~ 60% failure stress), as shown in Figure 2, which indicates that the rock is more heterogeneous with probably many pre-existing microcracks in it. Upon further loading, both the rocks showed distinctly different dilatant behaviour (Figures 1 and 2). The basalt suffered relatively less damage (Figure 1) until 98% failure stress, whereas the migmatite gneiss showed considerable damage as inferred from the nonlinearity of its stress–volumetric strain behaviour (Figure 2). This implies that the newly formed microcrack population was relatively high and had a faster growth as the impending failure approached in migmatite gneiss. Further, rock fracturing is generally characterized by a fast transient phenomenon showing a high degree of nonlinearity before final failure, and the AE signatures can provide a better description of it.

### *Microcracking activity as inferred from AE statistics*

The origin and development of microcracking activity in rocks resulting in inelastic volumetric strain and

**Table 1.** Physical and mechanical properties of Latur basalt (depth 214 m) and migmatite gneiss (depth 580 m) of KLR-1

| Parameter | Sample no. LB-1 (massive basalt) | Sample no. A-1 (migmatite gneiss) |
|---|---|---|
| Physical properties | | |
| Density, $\rho$ (g/cm$^3$) | 2.922 | 2.825 |
| P-wave velocity, $V_P$ (m/s) | 5699 | 6149 |
| S-wave velocity, $V_S$ (m/s) | 3317 | 3432 |
| Mechanical properties | | |
| Uniaxial compressive strength (MPa) | 261.00 | 187.29 |
| Poisson ratio, $\nu$ | 0.265 | 0.226 |

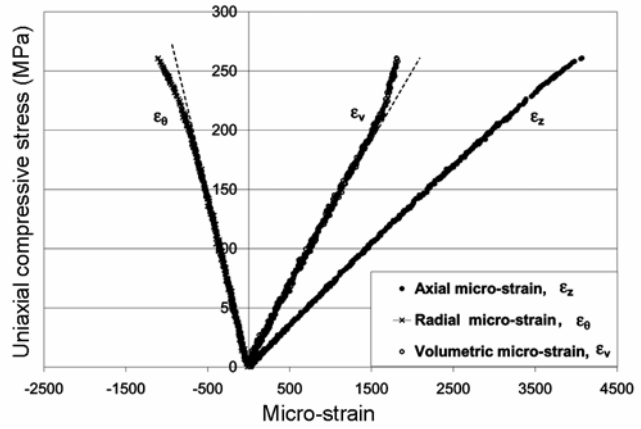


**Figure 1.** Stress–strain behaviour of sample no. LB-1 (massive basalt).

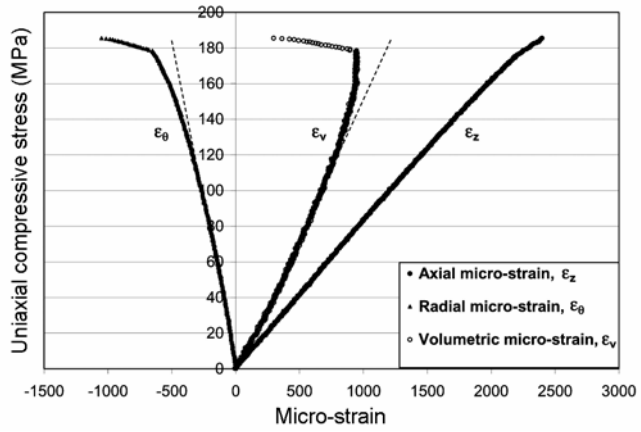


**Figure 2.** Stress–strain behaviour of sample no. A-1 (migmatite gneiss).

accompanying AE can be inferred from AE statistics, as the number of AE events is approximately proportional to the number of growing cracks and the AE amplitude or energy count data are proportional to the crack growth increments in rocks under compressive stress[11,12]. The most useful statistical parameters to identify, track and characterize the various stages of microcracking activity in the deforming rock have been found to be: (i) the occurrence rate of event and energy counts, (ii) amplitude distribution (*b*-value) and its stress-induced changes, (iii) cumulative energy or event counts as detailed in the following sections. The results of the present study as well as those reported earlier[9] show that there are three typical successive phases of microcracking activity, viz. primary, secondary and nucleation that would lead to the final failure of rocks under compression. The statistics of AE occurring during these phases as well as the sub-phases is distinctly different between the two rocks (Table 2), which also includes the energy per event ratio data of each sub-phase.

## *Frequency of occurrence*

The AE event rate, $\dot{\mathbf{n}} = \mathrm{d}n/\mathrm{d}t$ gives the simplest measurement of the frequency of microcracking activity. The energy associated with individual AE events would indicate the magnitude or energy of the microcrack ($\dot{\mathbf{E}}$) and the energy release rate, $\dot{\mathbf{E}} = \mathrm{d}E/\mathrm{d}t$ is a measure of the size distribution of microcracks in the deforming rock. The samples tested are of two different sizes, as mentioned above. Accordingly, the time taken for the final failure for the massive basalt, LB-1 (dia. 54 mm) was 670 s from the start of the experiment, whereas it was 510 s for the migmatite gneiss, A-1 (dia. 42 mm). During the initial stages of loading and elastic deformation, there was hardly any AE activity in terms of energy per event or ring down count (RDC) per event for LB-1, whereas it was present to some extent for sample A-1 (Table 2). In response to the formation of new microcracks, both the rocks began to generate AE at a steadily increasing rate. It had commenced at 440 s (~ 65% failure stress) after the start of the experiment for LB-1 and rather early at 260 s (~ 50% failure stress) after the start of the experiment for A-1. From then onwards, with the increase of stress until final failure, a large number of AE events from tens to several thousands were found to occur from both the rock samples with differences in details such as the occurrence rate and cumulative count data of AE parameters (events, RDC and energy). Therefore, the AE event rate ($\dot{\mathbf{n}}$) and energy release rate ($\dot{\mathbf{E}}$), which can provide direct

**Table 2.** Acoustic emission statistics during various stages of microcrack damage suffered by Latur basalt and migmatite gneiss that are stressed to fracture under uniaxial compression

| Stage | Failure time (normalized) | Failure stress (%) | Event count | Ring down count | Energy count | Energy per event | Microcrack damage (normalized) |
|---|---|---|---|---|---|---|---|
| Massive basalt (sample no. LB-1), depth = 214 m, dia. = 05.440 cm, length = 11.200 cm | | | | | | | |
| Pre-primary | 0–0.675 | 0–66.54 | 3,250 | 23,000 | 5,000 | 1.54 | 0–0.0035 |
| Primary-1 | 0.675–0.866 | 66.54–87.97 | 25,000 | 136,000 | 37,500 | 1.50 | 0.0035–0.0352 |
| Primary-2 | 0.866–0.896 | 87.97–90.98 | 7,300 | 98,000 | 68,000 | 9.32 | 0.0352–0.0952 |
| Secondary-1 | 0.896–0.970 | 90.98–98.50 | 14,600 | 160,000 | 85,000 | 5.82 | 0.0952–0.18 |
| Secondary-2 | 0.970–0.985 | 98.50–100 | 2,500 | 52,000 | 34,000 | 13.60 | 0.18–0.215 |
| Nucleation | 0.985–1.00 | 100–100 | 720 | 49,000 | 828,000 | 1150 | 0.215–1.000 |
| Migmatite gneiss (sample no. A-1), depth = 580 m, dia. = 04.19 cm, length = 09.44 cm | | | | | | | |
| Pre-primary | 0–0.654 | 0–66.31 | 700 | 18,600 | 3,400 | 4.86 | 0–0.016 |
| Primary-1 | 0.654–0.815 | 66.31–81.82 | 3,000 | 116,000 | 22,500 | 7.50 | 0.016–0.129 |
| Primary-2 | 0.815–0.854 | 81.82–86.10 | 1,300 | 46,500 | 16,600 | 12.77 | 0.129–0.211 |
| Secondary-1 | 0.854–0.955 | 86.10–95.72 | 4,150 | 132,000 | 98,500 | 9.28 | 0.211–0.361 |
| Secondary-2 | 0.955–0.971 | 95.72–97.33 | 6,000 | 200,000 | 72,000 | 12 | 0.361–0.495 |
| Nucleation | 0.971–1 | 97.33–100 | 350 | 11,200 | 14,400 | 41.14 | 0.495–1.000 |

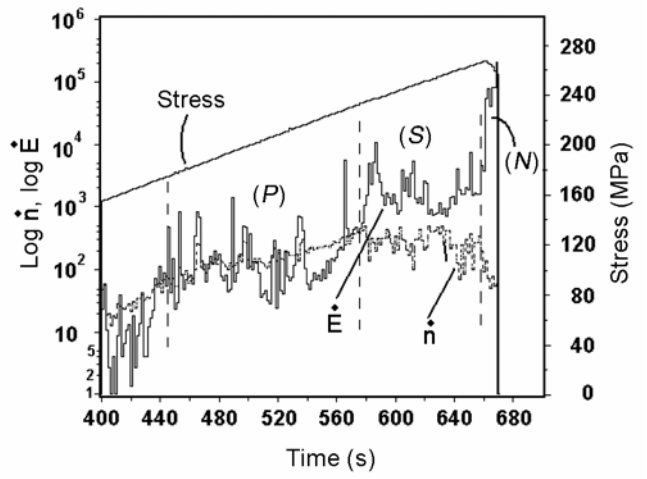


**Figure 3.** The stress and occurrence rate of acoustic emission (AE) event ($\dot{\mathbf{n}}$) and energy count ($\dot{\mathbf{E}}$) data obtained during the experiment on massive basalt (LB-1) plotted as a function of time to failure. P, S and N denote the primary, secondary and nucleation stages of microcrack damage suffered by the rock.

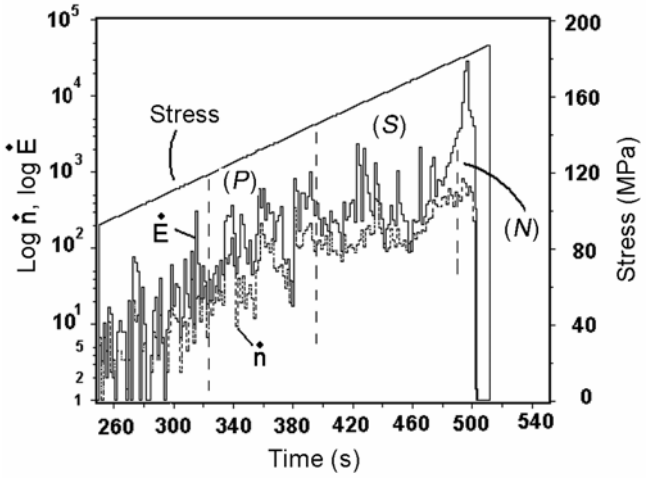


**Figure 4.** The stress and occurrence rate of AE event ($\dot{\mathbf{n}}$) and energy count ($\dot{\mathbf{E}}$) data obtained during the experiment on migmatite gneiss (A-1) plotted as a function of time to failure. P, S and N denote the primary, secondary and nucleation stages of microcrack damage suffered by the rock.

information on the frequency of microcracking activity in rocks, are plotted as a function of time in the logarithmic scale in Figures 3 and 4, for the massive basalt (LB-1) and migmatite gneiss (A-1) respectively. The plots were obtained as a function of time-to-failure at a fixed 200 bin digitization rate, which corresponded to the occurrence rate of AE for every 3.5 s for LB-1 and 2.5 s for A-1. These plots have helped identify the various stages or phases of prefailure microcracking activity in rocks and to filter (or window) the subsets of AE data for detailed analysis of each stage/phase. The related stress–time plot is also included in both the figures for a better evaluation. In general, the two AE parameters ($\dot{\mathbf{n}}$ and $\dot{\mathbf{E}}$) are found to show an increasing trend with the increase of stress (time) at different rates between the rocks and also with some fluctuations until the impending failure approached in the rock. The fluctuations of $\dot{\mathbf{E}}$ and $\dot{\mathbf{n}}$ were relatively small for the massive basalt (LB-1) compared to those of migmatite gneiss (A-1), which indicates that the density and size distribution of the newly formed microcracks in LB-1 are rather uniform and small, taking into account the RDC and energy count data of AE (Table 2). The relatively large fluctuations of the occurrence rate of AE in sample A-1 indicate that the rock has a heterogeneous structure. The statistics of other AE parameters also lends support to this observation, as discussed in the sections that follow. The present experimental results show that the microcracking activity occurs in three phases: primary, secondary and nucleation, which are in close agreement with the results reported by us earlier[9]. These three phases, which are identified from the plots of the present study, are shown in Figures 3 and 4. Both the parameters show a steady increase during the primary phase (*P*), remain nearly stable with small fluc-

tuations in the secondary phase (*S*), followed by an exponential increase of energy release rate ($\dot{\mathbf{E}}$) and a sharp fall of event rate ($\dot{\mathbf{n}}$) during the nucleation phase (*N*), as can be seen in Figures 3 and 4. The primary phase reflects the formation of new microcracks and their initial activity as revealed by an increase in event and energy release rate of AE in both the rocks. The secondary phase involves subcritical growth, of the microcrack population, as revealed by a smaller increase in event and energy rate of AE events with more or less equal amplitude (*b*-value), which are similar to the results reported by us earlier[9,25]. The nucleation phase corresponds to the initiation of accelerated growth of microcracks of higher amplitude and duration (or energy) leading to the ultimate macroscopic fracture along one or more incipient fracture planes. The duration of the nucleation phase was relatively small for LB-1 compared to A-1. Besides the frequency of occurrence of microcracking activity, the rocks of the present study show sharp differences in AE *b*-values and energy count data that are discussed below.

### *Size distribution*

Microcracks of different sizes (or AE of different peak amplitudes) are produced during rock fracture under compression. The most useful way of obtaining quantitative information on it is by computing the *b*-values of AE using the methods adopted in seismology[1,22]. The *b*-value is defined as the log-linear slope of the frequency–magnitude distribution of AE[10–14]. In the present study, the *b*-values derived by applying the maximum likelihood method[22] using the discrete frequency–amplitude distribution data of individual subsets of AE are found to be distinctly different between the two rocks, especially during the primary and secondary stages (Figure 5). The *b*-value which is inversely proportional to the size distribution of microcracks is relatively high for LB-1 on account of a large number of microcracks (or AE) of predominantly low amplitude that are produced during its primary phase (Figure 5). But the *b*-value dropped from 3.00 to 1.75 as the number of microcracks of relatively high amplitude began to occur during the secondary stage of LB-1. On the other hand, the migmatite gneiss (A-1) gave rise to smaller number of (microcracks) of relatively higher amplitudes during the primary and secondary phases, as inferred from the AE *b*-value that began to drop from 1.45 to 1.00 during the primary phase, and from 1.00 to 0.50 during the secondary phase (Figure 5, Table 2). However, during the nucleation phase, especially for LB-1, a sharp fall in *b*-value due to a surge of AE events of higher amplitude took place. Whereas in migmatite gneiss, the drop in *b*-value during the nucleation phase is not so significant since it had already given rise to a large number of AE (microcracking activity) during its primary and secondary phases. The statistics data (energy per event) shown in Table 2 also lend support to this observation.

### *Cumulative microcrack damage*

A complete characterization of the AE signal can be obtained by the RDC data, which is a measure of the number of AE waveform oscillations through a pre-set threshold voltage, and the 'energy counts', which is a measure of the area under the rectified AEs signal of transient nature. A large population of AEs with varying duration and amplitude occur during the deformation and failure of brittle rocks. The common practice is to examine the cumulative RDC and energy count ($\Sigma E$) data plots for the identification and assessment of important stages of microcrack damage in rocks. In the present study, the cumulative RDC and energy count data plots obtained

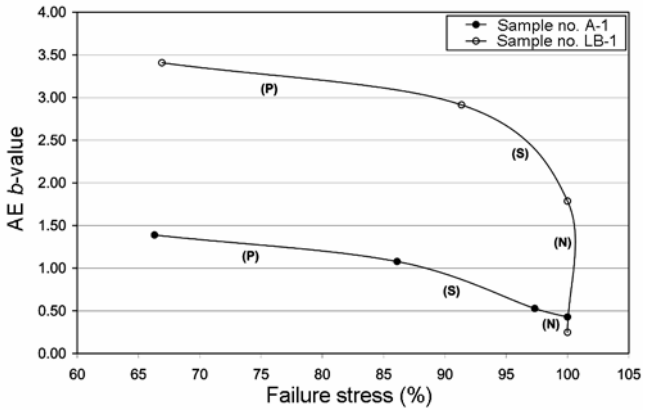


**Figure 5.** AE *b*-value versus failure stress (%) during the primary (*P*), secondary (*S*) and nucleation stage (*N*) of pre-failure damage for a massive basalt (LB-1) and migmatite gneiss (A-1). The *b*-values were computed using the maximum likelihood method[22,23] and the amplitude–frequency data of AE of individual phases.

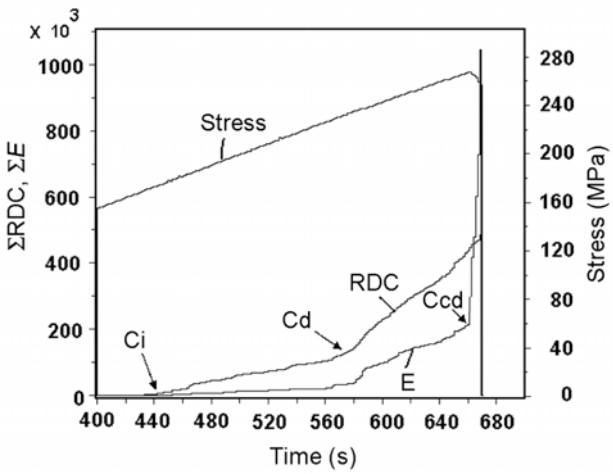


**Figure 6.** AE cumulative ring down count ($\Sigma$RDC) and energy count ($\Sigma E$) data as well as stress plotted as a function of time for a sample no. LB-1. The stages at which new microcracks initiate (Ci), cause damage (Cd) and critically damage (Ccd) as inferred from the plots are also marked in the figure. These correspond to the onset of primary, secondary and nucleation stages of pre-failure damage in the rocks.

during the replay of AE data are shown in Figures 6 and 7 for the massive basalt (LB-1) and migmatite gneiss (A-1) rock respectively. The plots obtained as a function of time starting from the onset time of dilatancy are shown in Figures 6 and 7. The time (or stage) at which new microcracks initiate (Ci) and cause damage (Cd) in the rocks could be identified easily from the RDC plots (Figures 6 and 7). It appears that the damage had commenced when the cumulative RDC was about 120,000 for LB-1 and 220,000 for A-1, indicating that AE events of longer duration were relatively more in A-1. Subsequently, the increase in RDC was relatively smooth until ~ 450,000 in LB-1, while it continued to increase sharply in A-1 until its final failure, implying that events of longer duration were relatively more in A-1. But as the impending failure was approaching fast, i.e. at the onset of crack critical damage (Ccd), it appears that the massive basalt (LB-1) had generated more number of events of longer duration (RDC) and higher energy or amplitude compared to the migmatite gneiss (A-1), as can be seen from the $\Sigma E$ versus time plot, and the statistics of energy per event data (Table 2). The three stages (Ci, Cd and Ccd) that have been identified from Figures 6 and 7 would correspond respectively, to the primary (*P*), secondary (*S*) and nucleation (*N*) phases of the prefailure damage in the rocks.

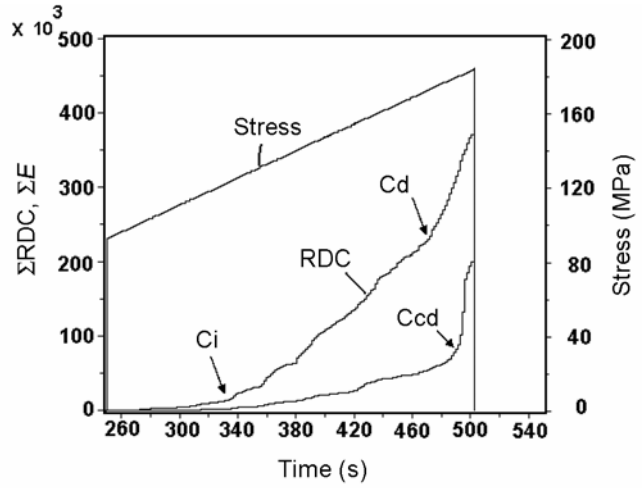


**Figure 7.** AE cumulative ring down count (∑RDC) and energy count ($\Sigma E$) data as well as stress plotted as a function of time for sample no. A-1. The stages at which new microcracks initiate (Ci), cause damage (Cd) and critically damage (Ccd) as inferred from plots are also marked in the figure. These correspond to the onset of primary, secondary and nucleation stages of pre-failure damage in the rocks respectively.

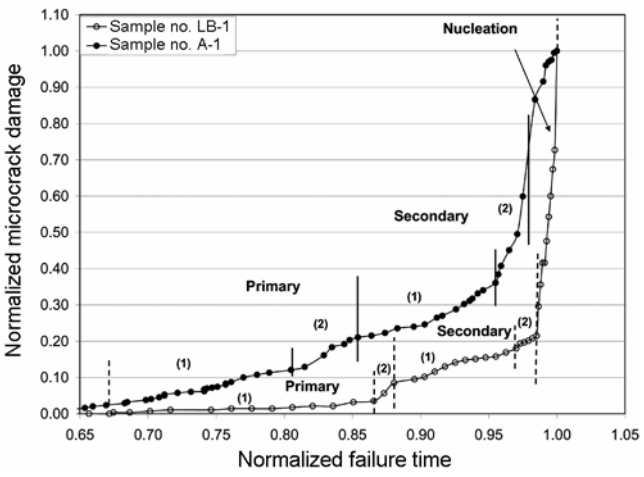


**Figure 8.** Normalized values of microcrack damage calculated from the cumulative AE energy count data are plotted as a function of time (normalized failure time) for samples LB-1 (massive basalt) and A-1 (migmatite gneiss). The sub-phases of the primary and secondary phases of microcrack damage that are inferred from the data are also marked in the figure.

### *Normalized microcrack damage*

The AE energy count represents the extent of microcrack damage both in terms of number as well as size of the microcracks that occur during the deformation of the rocks. Therefore, the cumulative energy count ($\Sigma E$) data are a fairly good measure of the microcrack damage that accumulates in the deforming rock. When normalized with respect to the final $\Sigma E$ count value at failure and plotted against the stress (or normalized failure time), it can help in identifying, tracking and also characterizing the various stages of normalized microcrack damage (*D*) right from the beginning (i.e. $D = 0$) until the final failure ($D = 1$) occurs in the rocks. The results of the present study are shown in Figure 8. The plots have been helpful to identify all the three main phases as well as the subphases of microcracking activity on the basis of sharp changes that have been noticed in the slopes of the data curves. The results show that the migmatite gneiss (A-1) had suffered more microcrack damage right from the beginning of the primary phase (*P*) compared to the massive basalt (LB-1). During the first part of the secondary phase (*S*), the normalized microcrack damage increased from 20% to 35% for A-1, and from 10% to only 18% for LB-1, which is approximately half of the damage suffered by A-1 (Figure 8). The microcrack damage increased sharply from the second part of the secondary phase (*S*) itself, to reach ~ 70% of normalized damage for the migmatite gneiss A-1. The rock had yielded more number of AE events of longer duration or RDC and higher amplitude (Table 2), whereas the massive basalt (LB-1) suffered extensive damage only during the nucleation phase (*N*) from 20% to 100% (Figure 8), as inferred from a heavy surge of AE events of higher energy and RDC (Table 2).

## Conclusion

The results of an experimental study of strength, deformation and failure behaviour of a massive basalt and a migmatite gneiss that represent the basalt cover and the Archaean granite–gneiss basement respectively, of Latur (KLR-1) are reported here.

Microcracking activity, as inferred from AE, and which occurred in a phased manner in both the rocks during the pre-peak stress regime had undergone a significant change in an accelerated manner with regard to the frequency of occurrence, size distribution and energy of individual microcracks as the impending failure was approaching at stresses close to failure.

The pre-failure microcracking was relatively small and homogeneous in the massive basalt compared to the migmatite gneiss during the primary as well as secondary phases. However, the nucleation phase commencing at ~98.5–99% failure stress in the massive basalt gave rise to more significant damage than the migmatite gneiss in which the nucleation phase started at lower stress, i.e. ~97% failure stress.

The results show that AE *b*-value and energy count data are more useful to characterize the failure behaviour of rocks and also to clearly identify the onset, track and analyse the nucleation phase of the final faulting and its growth in rocks under stress.


1. Scholz, C. H., The frequency–magnitude relation of microcracking in rock and its relation to earthquakes. *Bull. Seis. Soc. Am*., 1968, **58**, 399–415.
2. Locker, D. A., Berlet, J. D., Kuksenko, V., Ponomarev, A. and Sidorin, A., Quasi-static fault growth and shear fracture energy in granite. *Nature*, 1991, **350**, 39–42.
3. Lockner, D. A., The role of acoustic emission in the study of rock fracture. *Int. J. Rock Mech. Min. Sci. Geomech. Abstr*., 1993, **30**, 883–899.
4. Rao, M. V. M. S. and Kusunose, K., Failure zone development in andesite as observed from acoustic emission locations and velocity changes. *Phys. Earth. Planet. Interiors*, 1995, **88**, 131–143.
5. Satoh, T., Shivakumar, K., Nishizawa, O. and Kusunose, K., Precursory localization and development of microfractures along the ultimate fracture plane in amphibolite under triaxial creep. *Geophys. Res. Lett*., 1996, **23**, 865–868.
6. Lei, X. L., Nishizawa, O., Kusunose, K. and Satoh, T., Fractal structure of the hypocenter distribution and focal mechanism solutions of AE in two granites of different grain size. *J. Phys. Earth*, 1992, **40**, 617–634.
7. Lei, X. L., Kusunose, K., Rao, M. V. M. S., Nishizawa, O. and Satoh, T., Quasi-static fault growth and cracking in homogeneous brittle rock under triaxial compression using acoustic emission monitoring. *J. Geophys. Res. B*, 2000, **105**, 6127–6139.
8. Lei, X. L. *et al.*, Detailed analysis of acoustic emission activity during catastrophic fracture of faults in rocks. *J. Struct. Geol*., 2004, **26**, 247–258.
9. Lei, X. L., Satoh, T., Nishizawa, O., Kusunose, K. and Rao, M. V. M. S., Modeling damage creation in stressed brittle rocks by means of acoustic emission. In Controlling Seismic Risk, Proceedings of 6th International Symposium Rockbursts and Seismicity in Mines (eds Potrin, Y. and Hudyma, M.), Australia, March 2005, pp. 327–334.
10. Cox, S. J. D. and Meredith, P. G., Microcrack formation and material softening in rock measured by monitoring acoustic emissions. *Int. J. Rock Mech. Min. Sci. Geomech. Abstr*., 1993, **30**, 11–24.
11. Main, I. G., Meredith, P. G. and Jones, C., A reinterpretation of the precursory seismic *b*-value anomaly from fracture mechanics. *Geophys. J*., 1989, **96**, 131–138.
12. Main, I. G., Sammonds, P. R. and Meredith, P. G., Application of modified Griffith criterion to the evolution of fractal damage during compressional rock fracture. *Geophys. J. Int*., 1993, **115**, 67–80.
13. Sun, X., Hardy Jr, H. R. and Rao, M. V. M. S., Acoustic emission monitoring and analysis procedures utilized during deformation studies of geologic materials. In *Acoustic Emission: Current Practice and Future Directions* (eds Sachse, W., Roget, J. and Yamaguchi, K.), ASTM Publ., Philadelphia, 1991, pp. 365–380.
14. Rao, M. V. M. S., Significance of AE based *b*-value in the study of progressive failure of brittle rock: Some examples from recent experiments. In Trends in NDE Science and Technology. Proceedings 14th World Conference on Non-Destructive Testing, New Delhi, India, December 1996 (eds Nair, C. G. K. *et al.*), Oxford & IBH Publ, New Delhi, 1996, pp. 2463–2467.
15. Gupta, H. K., The deadly Latur earthquake. *Science*, 1993, **262**, 1666–1667.
16. Gupta, H. K. *et al.*, Investigation of Latur earthquake of 29 September 1993. *Geol. Surv. India Spec. Publ*., 1995, **27**, 17–40.
17. Rajendran, C. P., Rajendran, Kusala and John, Biju, The 1993 Killari (Latur), Central India, earthquake: An example of fault reactivation in the Precambrian crust. *Geology*, 1996, **24**, 651–654.
18. Gupta, K., Rastogi, B. K., Indra Mohan, Rao, C. V. R. K., Sarma, S. V. S. and Rao, R. U. M., An investigation into the Latur earthquake of 29 September 1993 in southern India. *Tectonophysics*, 1998, **287**, 299–318.
19. Pandey, O. P., Chandrakala, K., Parthasarathy, G., Reddy, P. R. and Koti Reddy, G., Upwarped high velocity mafic crust, Subsurface tectonics and causes of intra plate Latur–Killari (*M* 6.2) and Koyna (*M* 6.3) earthquakes, India – a comparative study. *J Asian Earth Sci*., 2009, **34**, 781–795.
20. Nagaraja Rao, G. M., Murthy, C. R. L. and Raju, N. M., Characterization of micro- and macro-cracks in rocks by acoustic emission. In *Acoustic Emission: Standards and Technology Update* (ed. Vahaviolos, S. J.), ASTM Spl. Tech. Publ., USA, 1998, p. 1353.
21. Rao, M. V. M. S., Murthy, D. S. N., Nagaraja Rao, G. M., Mohanty, S. K. and Udaya Kumar, S., Stress-induced microcracking and brittle failure of Godhra granite. *J. Geol. Soc. India*, 2004, **64**, 775–783.
22. Aki, K., Maximum likelihood estimates of *b* in the formula $\log N = a - bm$ and its confidence limits. *Bull. Earthquake Res. Inst., Tokyo Univ*., 1965, **43**, 237–239.
23. Rao, M. V. M. S., Determination and analysis of *b*-value of acoustic emission using different methods: A case study. *J. Nondestruct. Test. Eval*., 2003, **2**(3), 24–28.
24. Rao, M. V. M. S. and Prasanna Lakshmi, K. J., Amplitude distribution analysis of acoustic emissions and investigation of the development of brittle fracture in rock. *Indian J. Pure Appl. Phys*., 2006, **44**, 820–825.
25. Rao, M. V. M. S., Nagaraja Rao, G. M., Prasanna Lakshmi, K. J., Chary, K. B. and Vijay Kumar, K., Micro-cracking and brittle failure of some metamorphic and igneous rocks under compression: a laboratory study using AE. *J. Nondestruct. Test. Eval*., 2009, **8**(1), 17–23.


ACKNOWLEDGEMENTS. M.V.M. thanks Council of Scientific and Industrial Research, New Delhi for the grant of Emeritus Scientist position and financial assistance to carry out this work. We are grateful to the Director, National Geophysical Research Institute, Hyderabad and Director, National Institute of Rock Mechanics, Kolar Gold Fields for extending all the facilities and support.

Received 27 September 2010; accepted 7 June 2011